Rapid light-induced activation of retinal microglia in mice lacking Arrestin-1

CrossMark

Emily S. Levine [a], Azhar Zam [a], Pengfei Zhang [a], Alina Pechko [b], Xinlei Wang [a], Paul FitzGerald [a], Edward N. Pugh Jr. [a,c], Robert J. Zawadzki [c], Marie E. Burns [a,b,c,*]

[a] Dept. of Cell Biology and Human Anatomy, University of California Davis, Davis, CA 95618, United States
[b] Center for Neuroscience, University of California Davis, Davis, CA 95618, United States
[c] Center for Ophthalmology & Vision Science, University of California Davis, Davis, CA 95618, United States

A B S T R A C T

Microglia dynamically prune synaptic contacts during development, and digest waste that accumulates in degeneration and aging. In many neurodegenerative diseases, microglial activation and phagocytosis gradually increase over months or years, with poorly defined initial triggering events. Here, we describe rapid retinal microglial activation in response to physiological light levels in a mouse model of photoreceptor degeneration that arises from defective rhodopsin deactivation and prolonged signaling. Activation, migration and proliferation of microglia proceeded along a well-defined time course apparent within 12 h of light onset. Retinal imaging in vivo with optical coherence tomography revealed dramatic increases in light-scattering from photoreceptors prior to the outer nuclear layer thinning classically used as a measure of retinal neurodegeneration. This model is valuable for mechanistic studies of microglial activation in a well-defined and optically accessible neural circuit, and for the development of novel methods for detecting early signs of pending neurodegeneration in vivo.

© 2014 Elsevier Ltd. All rights reserved.

1. Introduction

In healthy neural tissue, microglia are dynamic, highly ramified cells that monitor their microenvironment and prune neural processes to maintain synaptic homeostasis (reviewed in Aguzzi, Barres, & Bennett, 2013; Kettenmann, Kirchhoff, & Verkhratsky, 2013; Wong, 2013). In response to neuronal infection, injury, or degeneration, microglia are the first and often only responders to phagocytose debris and dying cells. If the disruption of the microenvironment is sufficiently severe, microglia become irreversibly activated, transform into a migratory amoeboid shape, and become capable of large-scale phagocytosis (Langmann, 2007). Overactive microglia, and the macrophages they recruit from the circulation, are thought to participate in the initiation or escalation of neurodegeneration (Hanisch & Kettenmann, 2007). Understanding the earliest stages of microglial activation and the molecular mechanisms that regulate their phagocytic activity is critical for defining the signals that activate them, and for potentially controlling reversible tissue damage.

In the retina, microglial activation accompanies light damage, optic nerve transsection, ischemia, and many inherited degenerations (Karlstetter, Ebert, & Langmann, 2010). In many such instances involving photoreceptor cell death, the transition from healthy to diseased state is difficult to discern due to the slow progression of aging or disease onset. An animal model has been needed whereby photoreceptor development and retinal circuitry can be maintained in a healthy state, but a controllable physiological stimulus can abruptly induce microglial changes. In such a model, the fundamental aspects of microglial activation, migration, proliferation, and phagocytosis, as well as the cause and effect relations of microglia and neural apoptosis, can be mechanistically investigated.

The rapid, light-dependent degeneration of photoreceptors in mice lacking Arrestin1 (Arr1$^{-/-}$) offers such a model. The biochemical mechanisms that transduce light into electrical signals in rods have been extensively studied (Burns & Pugh, 2010) and loss of regulatory factors like Grk1 (rhodopsin kinase; C.K. Chen et al., 1999) and Arr1 (visual arrestin; Xu et al., 1997) that deactivate the photoexcited G-protein coupled receptor, rhodopsin, has been shown to lead to retinal degeneration. Retinas of Arr1$^{-/-}$ mice born and reared in constant darkness initially have normal morphology, but undergo light-dependent photoreceptor degeneration (J. Chen

* Corresponding author at: Center for Neuroscience, University of California Davis, Davis, CA 95618, United States.

E-mail address: meburns@ucdavis.edu (M.E. Burns).

et al., 1999) within days of exposure to bright light (Burns et al., 2006). The concurrent loss of the rod G protein alpha subunit (Gnat1), which is essential for downstream rhodopsin signaling, rescues rods of Arr1$^{-/-}$ mice from degeneration triggered by dim light (Hao et al., 2002). This finding supports the idea that photoreceptor cell death arises from excessive phototransduction signaling; however, the cellular and physiological mechanisms by which excessive signaling leads to degeneration remain unknown.

Here we show that Arr1$^{-/-}$ retinas exhibit dramatic light-dependent activation of microglia within hours of light exposure. Exposure to even dim light causes microglia to infiltrate the outer nuclear layer and engulf photoreceptor somata. Microglial activation is preceded by a dramatic increase in the light scattering of the photoreceptor layer observed *in vivo* by OCT imaging, revealing this non-invasive imaging modality as a means for detecting cell stress far before classic measures of degeneration are apparent. Thus, the Arr1$^{-/-}$ mouse is an exciting model for studying the acute, physiological induction of microglial activation and the earliest stages of photoreceptor cell death. This system is also valuable for development of *in vivo* metrics of neural stress prior to degeneration and for testing interventions that could reverse the microglial activation.

2. Materials and methods

2.1. Use of animals

Mice were cared for and handled in accordance with National Institutes of Health guidelines for the care and use of experimental animals and approved protocol by the Institutional Animal Care and Use Committee of the University of California, Davis in accordance with the Code of Ethics of the World Medical Association (Declaration of Helsinki) for experiments involving humans. Adult wild type C57BL/6J (Jackson Laboratory) were used as control mice. Mice were reared in 24-h darkness, or in the case of a subset of WT mice, reared in cyclic light and dark-adapted overnight prior to experimental light exposure. Mice kept in uniformly illuminated plastic enclosures were either exposed to standard cyclic light with an intensity of ~25 lux for up to 168 h, constant light with an intensity of ~200 lux for up to 96 h, or a brief light with an intensity of ~5000 lux for 2 min followed by up to 72 h in darkness. The intensity of the illumination was measured at the floor of the enclosure with a calibrated meter in photopic lux (lumens m^{-2}). Assuming that the undilated pupils of the mice contracted to a diameter of 0.3 mm, the retinal light flux and rate of rhodopsin isomerization (R^* rod^{-1} s^{-1}) can be determined (Lyubarsky, Daniele, & Pugh, 2004). Assuming perfect homogeneity, the illumination producing 25 lux illumination at the pupil plane excited ~250 R^* rod^{-1} s^{-1} across the retina, 200 lux generated ~2000 R^*-rod^{-1} s^{-1}, and 5000 lux generated ~50,000 R^* rod^{-1} s^{-1}. The Arr1$^{-/-}$ mice were originally described in Xu et al. (1997), and displayed indistinguishable light responses to those originally described (data not shown). Gnat1$^{-/-}$ mice were originally described in Calvert et al. (2000) and crossed with the Arr1$^{-/-}$ line to homozygosity. The WT, Gnat1$^{-/-}$ and Arr1$^{-/-}$ mice used in these specific experiments were screened for the rd8 mutation (Mattapallil et al., 2012) and found to be lacking the mutation (data not shown).

2.2. Immunohistochemistry

Mice were euthanized by CO_2 narcosis and decapitated, and the eyes were removed and immersed in 4% paraformaldehyde in phosphate buffered saline (PBS) for 5 min at room temperature. The anterior segments were then cut away, the lens removed, and the eyecups fixed for 20 additional minutes. Eyecups were stored in 1× PBS at 4 °C until sectioning. Eyecups were embedded in low-melting agarose (Invitrogen, Cat. #18300-012) preheated to 70 °C and oriented so as to cut planar to the dorsoventral midline as described in Daniele et al. (2011) and Wagner, McCaffery, and Dräger (2000). 150 μm-thick sections were made with a vibratome (Leica Microsystems, model VT 10005) and stored in small base molds of 1× PBS at 4 °C. Sections were incubated with normal sera (goat; Jackson ImmunoResearch) for about 1 h at room temperature. The sections were then incubated in primary antibodies at 4 °C overnight. After three 5 min washes in 1× PBS, secondary antibodies were applied for 1.5–2 h at room temperature. The sections were washed 3 times for 5 min each in 1× PBS, incubated in DAPI (Invitrogen Life Technologies,) then washed three additional times before being mounted onto slides in polyvinyl alcohol mounting medium with DABCO (Sigma Aldrich) or ProLong Gold Antifade Reagent (Invitrogen Life Technologies).

Primary antibodies used for immunohistochemistry include rabbit anti-Iba1 (019-19741; Wako) at a 1/500 dilution and rat anti-CD68 (MCA1957T; AbD Serotec) at a 1/1000 dilution. Alexa 488-conjugated goat anti-rabbit and Alexa 633-conjugated goat anti-rat (Invitrogen Life Technologies) were used as secondary antibodies at 1/300 dilution. Immunosera were diluted in a buffer of PBS with bovine serum albumin (0.5%) and Triton X-100 (0.5%).

Slide-mounted sections were visualized with a Nikon Ti-E A1 multiphoton imaging system using a 40×-water immersion objective and continuous wave lasers. Three-dimensional images (30 μm in Z) were sampled from the center and peripheral regions of each section using the NIS-Elements Microscope Imaging Software (Nikon). Cell numbers, morphological features, and layer thicknesses were counted and measured manually.

2.3. Cryosectioning and TUNEL staining

Retinas were fixed by freeze substitution as described in Yoon and FitzGerald (2009). Briefly, methanol–acetic acid fixative (97% methanol and 3% acetic acid) and propane were chilled to dry ice temperature in advance. Liquid propane was prepared by condensing gaseous propane in the walls of an aluminum PCR block chilled to dry ice temperature. Fresh eyes were rapidly dissected and immersed in liquid propane for 1 min, then transferred into chilled methanol–acetic acid fixative and stored at −80 °C for 48 h. After gradually warming to room temperature, tissue was rehydrated by immersion in fixative with 20%, 40%, 60%, and 80% 1× PBS for 10 min each, then in 100% 1× PBS overnight.

Following rehydration, eyes were embedded in OCT Compound (Tissue-Tek, Sakura, Tokyo, Japan), and cryosectioned at 16 μm thickness in the sagittal plane, allowing dorsal to ventral observation using Microm HM 550 cryostat (Thermo Scientific). Slices were cut adjacent to or through the optic nerve head to minimize variations in retinal thickness. Apoptotic cells were detected using Click-iT TUNEL Alexa Fluor 647 imaging assay (Invitrogen Life Technologies), according to the manufacturer's protocol. Briefly, frozen sections were permeated by 0.25% Triton X-100 in PBS for 20 min. Sections were incubated in a TdT reaction cocktail for 1 h at 37 °C, then protected from light in a Click-iT reaction cocktail for 30 min at room temperature. Sections were mounted with ProLong Gold Antifade Reagent with DAPI (Invitrogen Life Technologies) following incubation.

Slide-mounted sections were visualized with a Nikon Ti-E A1 multiphoton imaging system using a 40×-water immersion objective and continuous wave lasers. The mean intensities of DAPI (blue) and TUNEL (red) channels were measured from the outer nuclear layer from central and peripheral regions of each section. The ratio of red to blue intensities was calculated in order to normalize the TUNEL signal by the number of remaining nuclei as

degeneration progressed. Measurements of outer nuclear layer thickness were made at 3–5 different locations in order to compute the mean for that region. For each data point in Fig. 3D, 3–8 sections were sampled from 2 to 4 eyes.

2.4. Fd-OCT imaging

Mice anesthetized with 2–3% isoflurane were placed on a heating pad and the head positioned so that the optic disc of the retina was aligned in the center of the OCT scan. Pupils were dilated topically with a drop of 1% tropicamide and 2.5% phenylephrine, and corneas were kept hydrated by artificial teardrops (methyl cellulose) during imaging. A custom built OCT imaging system developed at the University of California, Davis (Alam et al., 2006; Kim et al., 2011; Zawadzki et al., 2005) equipped with CMOS camera (Basler) was used to acquire data at 50 k A-scans/s using a Super Luminescent Diode (SLD) as a short coherence light source with the spectrum centered at 855 nm and 132 nm bandwidth (Superlum). The instrument achieved axial resolution of about 3 μm and lateral resolution of about 4 μm in ocular tissue. OCT volumes (100 B-scans × 2000 A-scans/B-scan) spanning ∼0.9 mm × 0.9 mm at the retina (32 μm/deg) were acquired in each experimental session. Registration of images across sessions was achieved with OCT en face projections (fundus view reconstructed from OCT volumes), which reduced errors due to variability in the location and orientation of the mouse retina between measurements.

Hi-resolution B-scans (16 bit, linearly scaled intensity; 2000 A-scans/B-scan) were acquired sequentially from each eye of dark-reared WT and Arr1$^{-/-}$ mice at each time point. Within a given eye of an individual animal, thirty B-scans were averaged to reduce the speckle noise in the image, corresponding to lateral averaging over 10 μm. A semi-automated segmentation software developed at Duke University (Chiu et al., 2010; Lee et al., 2013) was used to calculate the thickness and average intensity of each layer. These measurements were made sequentially at the same eccentricity in the same animal over time, resulting in longitudinal data. For thickness analysis, the OPL and ONL were combined into a single layer because the two layers became indistinct during the time course of the degeneration in Arr1$^{-/-}$ retinas. For intensity analysis, the INL reflectance, which was unaffected by light exposure, was used to normalize the light scattering changes in the photoreceptor layers, removing small variations in absolute intensity across imaging sessions that might arise from subtle differences in alignment and other factors affecting image quality.

2.5. Electron microscopy

Retinas were fixed and prepared in a similar manner to that described in Daniele et al. (2011). Briefly, mice were asphyxiated with CO_2, and then euthanized by cardiac perfusion with a fixative of 2.5% glutaraldehyde, 2% paraformaldehyde in 0.1 M sodium cacodylate. Corneas and lenses were removed and a square centered on the optic disc was sliced from the back of the eyecups. Tissue was subjected to overnight fixation, submersed in 1% OsO_4, and embedded in PolyBed 812 resin after dehydration in graded ethanol. Thin sections were made with a Leica EM UC6 microtome and stained with either 3% uranyl acetate in 50% methanol or 4% uranyl acetate in 70% ethanol followed by 0.3% lead citrate. Images were taken with a transmission electron microscope (Philips CM120 Biotwin) and a digital camera (Gatacan MegaScan, model 794/20) at the University of California, Davis, School of Medicine, Department of Pathology and Laboratory Medicine, Electron Microscopy Lab, Davis, CA. Images were subsequently stitched together in Adobe Photoshop CS6.

3. Results

### 3.1. Two phases of microglial activation in light-exposed Arr1$^{-/-}$ retina

Microglia uniformly tile the healthy retina and extend highly branched processes that reside primarily within the synaptic layers, the outer plexiform (OPL) and inner plexiform (IPL) layers (Hume, Perry, & Gordon, 1983). In wild-type (WT) mice born and reared in constant darkness, the retinal microglia also ramify in these layers, indicating that the localization of resting microglia in the synaptic layers is normally independent of light-driven retinal activity (Fig. 1A, 0 h; Fig. 1B and C zero time point, black circles). The microglia of Arr1$^{-/-}$ mice reared in constant darkness showed this same ramification in the synaptic layers, and were comparable in number and distribution across the retina (Fig. 1A, 0 h; Fig. 1B and C zero time point). These results show that the loss of Arr1 expression in photoreceptors does not itself affect the native state of resting microglia.

Mice lacking Arr1 have greatly prolonged rod signaling and undergo light-dependent photoreceptor degeneration (J. Chen et al., 1999; Xu et al., 1997). To test whether light exposure also caused changes in retinal microglia, we exposed dark-reared WT and Arr1$^{-/-}$ mice to 200 lux white light and examined the distribution of microglia in the retina using an antibody to the microglial marker, Iba1. By 12 h after light onset, there was an abrupt and transient increase in the number of microglia extending processes radially across retinal layers (Fig. 1A and D). At this early time, there was no change in the *total* number of Iba1-positive cells in the retina (Fig. 1C), but a profound increase in the fraction of Iba1-positive cells located in the outer retina (Fig. 1B). These results are consistent with rapid migration, but not proliferation, of resident retinal microglia from the synaptic layers into the outer nuclear layer in response to light. Such light-dependent changes were not observed in WT mice (Fig. 1).

Between 36 and 72 h of continuous illumination, Arr1$^{-/-}$ retinas showed a dramatic 3.3-fold increase in the total number of Iba1-positive cells ($p < 10^{-8}$; Fig. 1C), suggesting either proliferation of resident microglia or infiltration of macrophages from the circulation. At this time, the Iba1-positive cells lacked highly branched processes and were amoeboid in shape (Fig. 1A); optical confocal sections through the outer nuclear layer revealed that many cells were engulfing photoreceptor somata (Fig. 1A and E). After 96 h illumination, Arr1$^{-/-}$ outer segments were no longer visible and round, Iba1-positive cells filled the otherwise empty space between the retina and the underlying retinal pigment epithelium layer. Nearly all of the large, round, Iba1-positive cells of Arr1$^{-/-}$ retinas also prominently stained for CD68, a marker of microglial activation, by 72 and 96 h (red; Fig. 1A). In WT mice, there was a small 1.5-fold increase in the total number of Iba1-positive cells between 36 and 72 h of light exposure ($p = 0.036$), but no significant changes in cell localization, morphology, or CD68 expression (Fig. 1).

The time course of microglial activation in Arr1$^{-/-}$ retinas was relatively insensitive to light intensity and depended more on the duration of exposure. For example, brief exposure to much brighter light (5000 lux, 2 min) caused no significant change in Iba1-positive cells of Arr1$^{-/-}$ retinas (blue triangles, Fig. 1B–E). In contrast, when the light was far dimmer and allowed to vary on a normal diurnal cycle (25 lux; 12L/12D; open green circles, Fig. 1B–E), we observed similar changes in Iba1-positive cell number, shape and migration to those seen under 200 lux constant illumination. Prevention of rod signaling by deletion of the rod alpha subunit of transducin (Arr1$^{-/-}$ Gnat1$^{-/-}$ mice) provided full rescue of the light-dependent changes in microglial activation and photoreceptor degeneration from 200 lux light exposure (red triangles, Fig. 1B–E). Together, these results show that retinal microglia
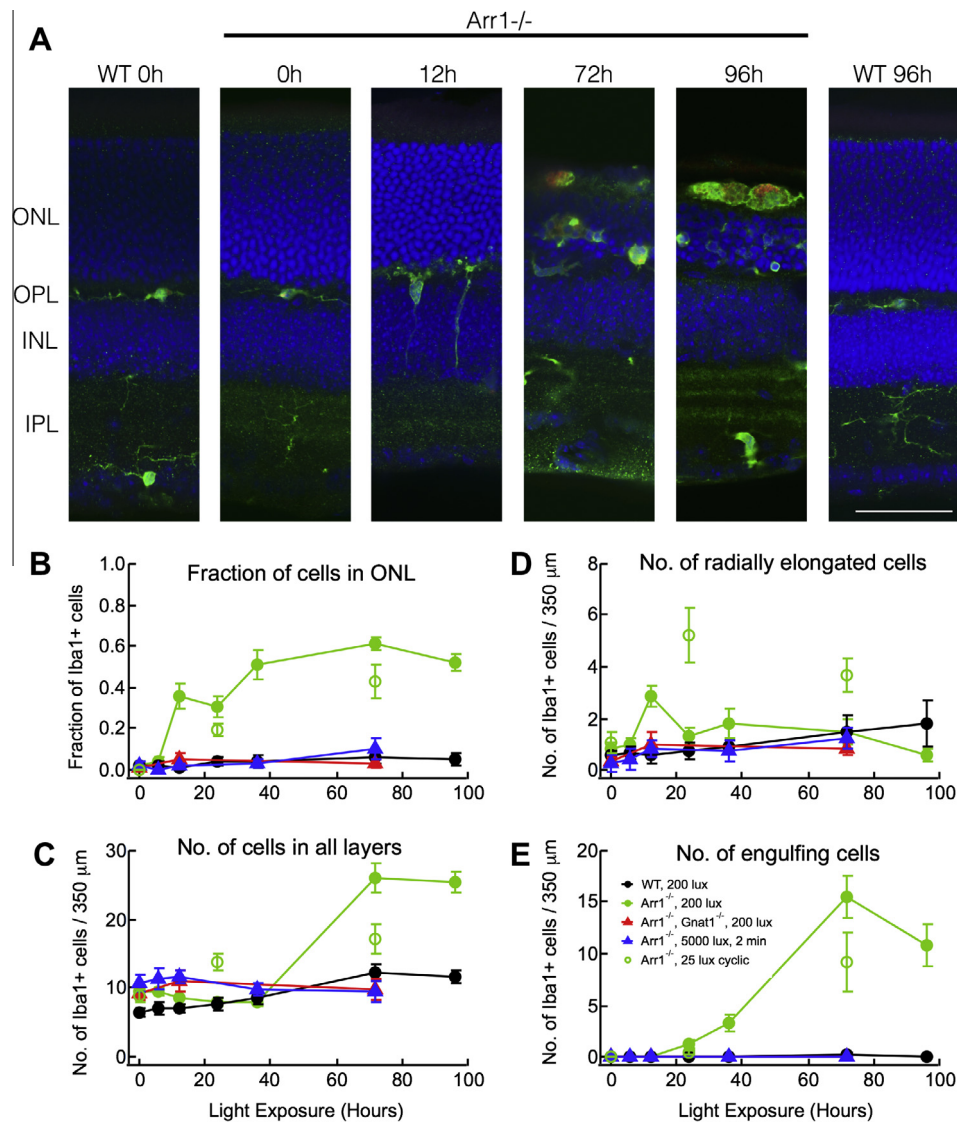
Fig. 1. Microglia are activated by dim light in Arr1$^{-/-}$ retinas. (A) Immunostaining of paraformaldehyde-fixed retinal sections of dark-reared WT and Arr1$^{-/-}$ mice after continuous light exposure (200 lux, estimated to produce 250 R*/s; Methods). Resting microglia (Iba1-positive, green) were initially confined to the plexiform layers (0 h), but after 12 h of light exposure extended processes radially towards and into the outer nuclear layer (ONL; DAPI, blue). By 72 h, microglia engulfed photoreceptor cell bodies and displayed increased CD68 staining (red), a sign of activation. Scale bar, 50 μm. Outer nuclear layer (ONL); outer plexiform layer (OPL); inner nuclear layer (INL); inner plexiform layer (IPL). (B–E) Quantification of the number and distribution of Iba1-positive cells in retinas of WT (black), Arr1$^{-/-}$ (filled green), or Arr1$^{-/-}$; Gnat1$^{-/-}$ (red), exposed to 200 lux continuous light. Arr1$^{-/-}$ mice exposed to 25 lux cyclic light (open green), or Arr1$^{-/-}$ mice exposed to 5000 lux for 2 min (blue). Error bars represent SEM.

respond rapidly to prolonged signaling in rod photoreceptors, rather than migrating into the ONL as a late consequence of degeneration.

3.2. Increased Arr1$^{-/-}$ photoreceptor light scattering in vivo portends degeneration

Common signs of neuronal stress, including pre-apoptotic cell condensation, mitochondrial swelling, and activity-dependent volume fluctuations, can produce local changes in optical refractive index. Such changes alter light scattering properties of the tissue, which can be detected with optical coherence tomography (OCT). In ophthalmological clinics worldwide, OCT imaging provides *in vivo* assessment of the layers of the retina, and is used to follow the course of ocular disease and treatment (Drexler & Fujimoto, 2008; Duker & Adhi, 2013). Recently, OCT measurement of increased light scattering has been proposed to indicate impending

cell death in the retina, though the underlying subcellular mechanisms that give rise to these changes have yet to be determined (Farhat et al., 2011; Mulvey et al., 2011; Van der Meer et al., 2010).

To examine whether photoreceptors of Arr1$^{-/-}$ mice show changes in optical scattering that could accompany microglial activation or signal early photoreceptor stress, we performed Fourier-domain (Fd)-OCT imaging from the same retinal area of dark-reared animals before and during light exposure (Fig. 2A). In WT mice, Fd-OCT images showed clear boundaries delineating the retinal layers, including the outer segments, inner segments, and cell bodies of the photoreceptors (outer nuclear layer, ONL) due to distinctive scattering properties of these layers (Fig. 2A and B). In dark-reared Arr1$^{-/-}$ animals that were imaged in darkness, the thicknesses and relative intensities of these boundaries were indistinguishable from those of WT (Fig. 2A and B), further confirming that dark-rearing protects Arr1$^{-/-}$ retinas from degeneration (Fig. 1 and C.K. Chen et al., 1999).
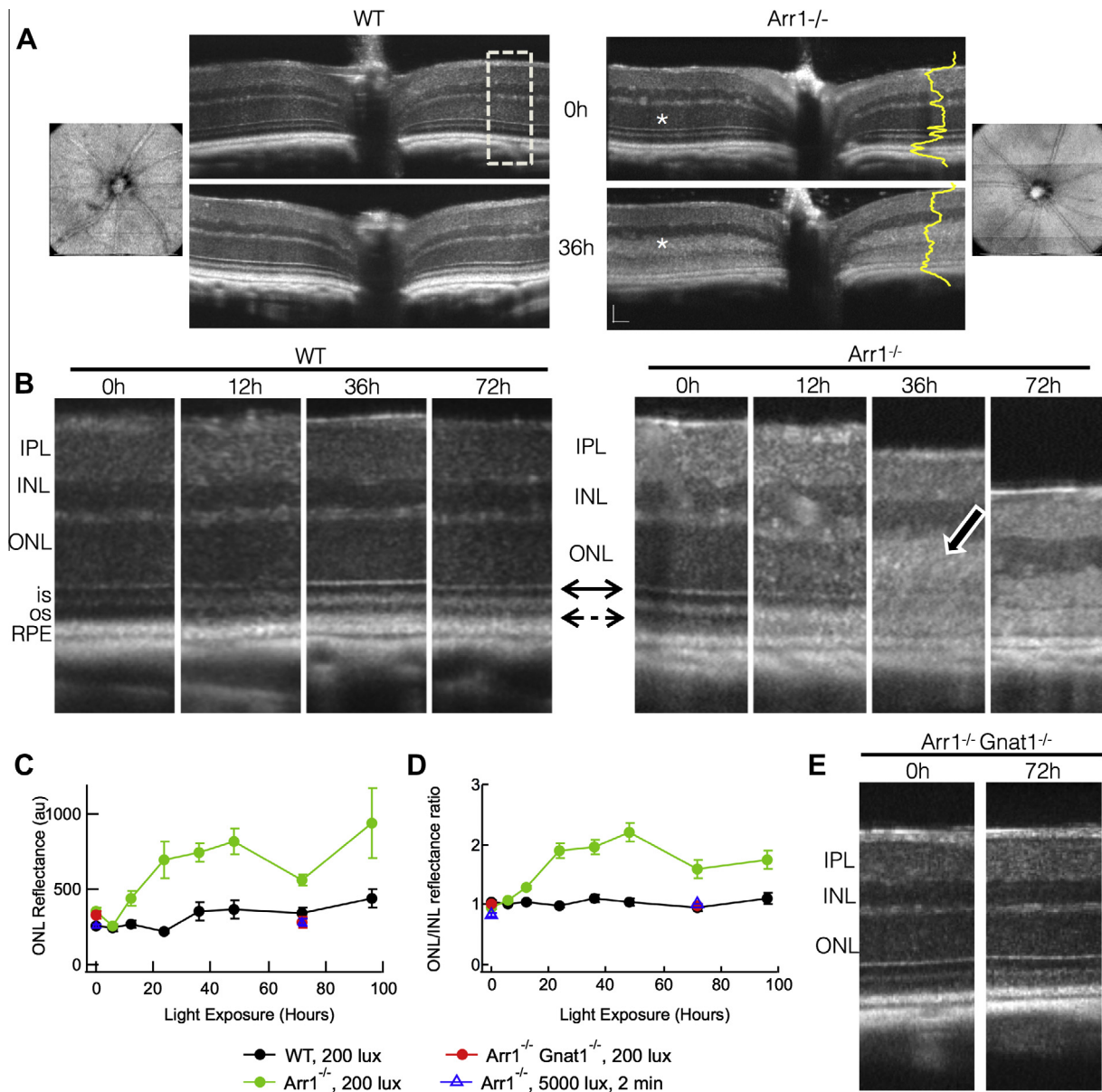
Fig. 2. Light-scattering and retinal layer boundary changes measured *in vivo* with OCT reveal early events in degeneration of Arr1$^{-/-}$ mice. (A) Fd-OCT images of a WT and an Arr1$^{-/-}$ mouse before and after 36 h of steady light (200 lux). The OCT imaging was centered on the optic disc. Blood vessels radiating from the optic disc seen in en face fundus views (leftmost and rightmost panel) did not change over time and were used for alignment in sequential sessions so that quantification could be performed on the same region. Dramatic increase in light scatter of the outer nuclear layer (ONL) was observed in all Arr1$^{-/-}$ mice exposed for at least 6 h of continuous illumination (white asterisks). Dashed box represents areas used for quantification of intensities across retinal layers (yellow) and magnified in B. Scale bar = 50 μm. (B) Higher magnification OCT scans from two representative animals over time. All Arr1$^{-/-}$ retinas showed loss of the external limiting membrane (solid double arrow) and increased intensity of the ONL (photoreceptor cell bodies; white bordered arrow). Dashed arrow points to the outer segments, which appear as the dark band between the reflective inner segment-outer segment border and the RPE. (C) Average reflectance of the ONL layer across animals measured from the pixel intensities across the retinal layers like those shown in yellow in (A). (D) Normalization of the ONL reflectance by that of the unchanging INL reduced variability across animals and imaging sessions. (E) No changes were observed in OCT scans of Arr1$^{-/-}$Gnat1$^{-/-}$ double knockout mice, which lack rod phototransduction signaling.

In response to steady 200 lux illumination, there were profound changes in the photoreceptor layers of Arr1$^{-/-}$ mice ($n = 26$ separate observations from both eyes of 6 different mice). By 12 h after light onset, the border between the outer segments and the retinal pigment epithelium (RPE) had become less distinct (dashed arrow, fig; Fig. 2B) and the reflectance of the ONL had increased (Fig. 2B–D). The reflectance of the ONL continued to increase over time (white bordered arrow; Fig. 2B), and was quantified by measuring the pixel intensities across the layers of the retina (Fig. 2C and D). At 36 h, the distinct border between the inner and outer segments and the sharp refractive boundary of the external limiting

membrane (solid double arrow) were much less apparent (Fig. 2B). The total thickness of the photoreceptor layers (from the distal border of the ONL to the proximal border of the RPE) decreased significantly by 36 h and continued to decline with time (Fig. 2B, see also Fig. 3E blue).

Such scattering and thickness changes were not observed in dark-reared WT mice ($n = 28$ separate observations in 6 different mice; Fig. 2B–D, black; Fig. 3E gray), indicating that these light-induced changes in scattering arose specifically as a consequence of Arr1 deletion. Likewise, changes in light scatter were not observed in Arr1$^{-/-}$ Gnat1$^{-/-}$ double knockout mice that lacked
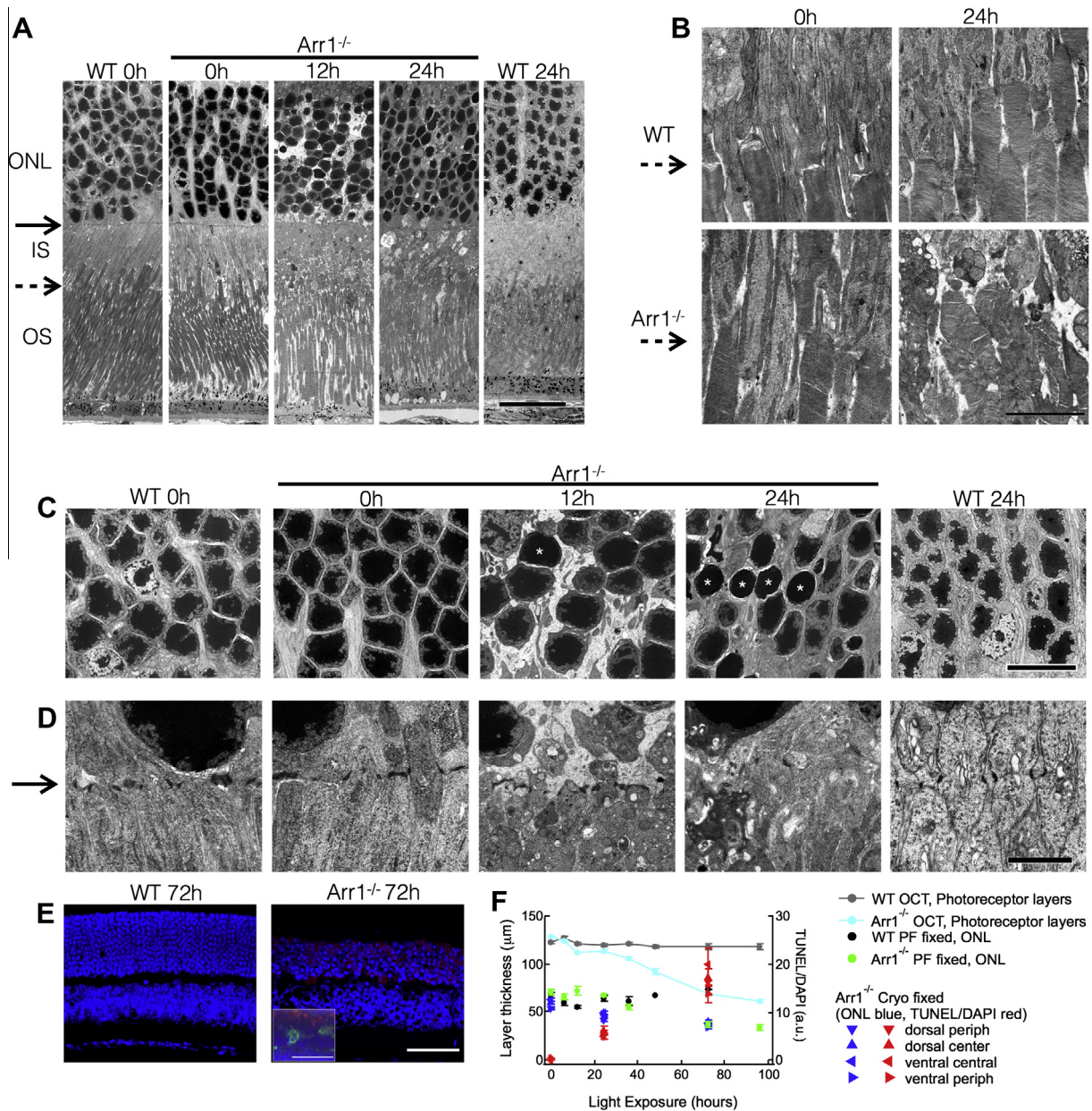
Fig. 3. Early ultrastructural changes in Arr1$^{-/-}$ photoreceptors after light exposure. (A) By 12 h, constant light exposure (200 lux) caused disappearance of the adherence junctions comprising the outer limiting membrane (solid arrows), inner segment vesiculation, and condensation of photoreceptor somata. (B) The inner segment-outer segment junction (dashed arrows) is normal in Arr1$^{-/-}$ mice before light exposure, but becomes severely disrupted after 24 h of constant light. (C) Light caused somatic swelling at 12 h that was accompanied by nuclear extrusions. By 12 h many nuclei were small and smooth (asterisks). (D) The electron dense tight junctions of Müller cell processes forming the external limiting membrane (solid arrow) vanished after 12 h of constant light exposure as the inner segments vesiculated in the Arr1$^{-/-}$. (E) TUNEL (red) and DAPI (blue) stained cryo-MeOH fixed thin sections. Inset shows paraformaldehyde-fixed thick section also immunostained for Iba1 (green). (F) Comparison of thickness measurements by OCT and common fixed sectioning techniques, and the time course of TUNEL-positive signals. Scale bars: (A) 20 µm; (B) 5 µm; (C) 10 µm; (D) 2 µm; (E) 50 µm. Outer nuclear layer (ONL); inner segments (IS); outer segments (OS).

phototransduction signaling (red; Fig. 2C and D), or in dark-reared Arr1$^{-/-}$ mice exposed to 5000 lux light for 2 min (blue triangles; Fig. 2C and D). These results suggest that the light-dependent changes in Arr1$^{-/-}$ retinas that are detectable by OCT, like the microglial activation described above, arise from prolonged rod signaling.

3.3. Cellular mechanisms underlying the light-scattering changes observed by OCT

To investigate the ultrastructural changes that might underlie the increased light scattering in Arr1$^{-/-}$ OCT images, we performed

transmission electron microscopy. Dark-reared WT and Arr1$^{-/-}$ photoreceptors were very similar in appearance (0 h; Fig. 3A), with inner and outer segments of comparable lengths and organization (dashed arrow indicates inner segment-outer segment boundary; Fig. 3A and B). In addition, the nuclei of WT and Arr1$^{-/-}$ ONL showed similar packing and chromatin staining (Fig. 3A and C), as well as comparable adherens junctions between Müller glia and photoreceptor inner segments, which comprise the external limiting membrane (solid arrow; Fig. 3A and D). After 12 h of light exposure, Arr1$^{-/-}$ outer segments remained normal in appearance and contained normal disc organization, but did not seem to be packed together as tightly as those of WT (Fig. 3A). In contrast, there were substantial ultrastructural changes within the inner

segments and cell bodies. The external limiting membrane was less regular in appearance (solid arrow; Fig. 3A and D), and the mitochondria of the inner segments appeared more numerous and less tubular (Fig. 3A and D). The photoreceptor nuclei were slightly swollen, displayed denser chromatin staining, and many exuded string-like structures (ONL; Fig. 3A, C, and D) resembling apoptopodia that have been shown to attract phagocytes (Poon et al., 2014).

After 24 h of light exposure, the photoreceptor inner segments appeared severely disrupted (Fig. 3A, B, and D), and the external limiting membrane was no longer discernible (solid arrow; Fig. 3A and D). Interestingly, the distal outer segments of Arr1$^{-/-}$ rods remained remarkably intact (Fig. 3A), while the inner segment-outer segment junction revealed substantial disorganization of the basal discs (dashed arrow; Fig. 3A and B). In addition, Arr1$^{-/-}$ photoreceptor somata were less densely packed, and there was a higher incidence of small, smooth rod nuclei with condensed chromatin (Fig. 3A and C white asterisks). Although WT photoreceptors showed light-dependent changes in mitochondrial shape and chromatin staining, they lacked all signs of disruption evident in the Arr1$^{-/-}$ retina (Fig. 3A–D).

The nuclear changes we observed by electron microscopy prompted us to investigate whether microglia infiltrating the ONL were selectively phagocytosing cells that had undergone chromatin fragmentation, a late sign of cell death. Using a standard terminal deoxynucleotidyl transferase dUTP nick end labeling (TUNEL) assay, we compared the time course and localization of TUNEL-positive signals to that of phagocytic Iba1-positive cells. TUNEL staining became apparent at the relatively late times that coincided with thinning of the ONL (Fig. 3E and F), but was not specifically associated with phagocytic Iba1-positive cells (Fig. 3E, inset). These results suggest activated microglia do not selectively target photoreceptors in the late stages of cell death.

4. Discussion

4.1. Prolonged rod signaling initiates two stages of microglial activation

Here, we describe two distinct stages of microglial activation that precede photoreceptor degeneration in the Arr1$^{-/-}$ mouse: migration and population growth. Under 12 h of room light (200 lux) in pigmented mice with un-dilated pupils, the microglia of Arr1$^{-/-}$ retinas dramatically change their appearance and localization, extending processes radially into the outer retina (Fig. 1A and D). The early increase in the number of microglia in the outer retina coincided with a reduction in the number of microglia in the inner retina (data not shown). This migratory phase persisted exclusively for at least 48 h (Fig. 1B); at much later times (72 h), the total number of Iba1-positive cells in the retina dramatically increased (Fig. 1C).

We are intentionally cautious in identifying the Iba1-positive cells as "microglia" in the initial migratory phase, and those cells in the second, proliferative phase as "Iba1-positive", because our experiments cannot distinguish between mitotic division of resident microglia or infiltration of macrophages from the circulation at late times. Previous studies have suggested that the increase in microglial cell number during light dependent retinal degeneration is primarily due to macrophage infiltration via the vitreous, choroid, and ciliary body (Joly et al., 2009; Karlstetter, Ebert, & Langmann, 2010; Santos et al., 2010). In contrast, neural damage in other brain regions produces mitotic expansion of microglial populations (Wirenfeldt et al., 2007). The extent to which proliferation contributes to the microglial population increase in cases of photoreceptor degeneration remains unclear (Santos et al., 2010).

Surprisingly, Arr1$^{-/-}$ mice exposed to a brief intense light (5000 lux, 2 min, estimated to produce 50,000 R* rod^{-1} s^{-1}, Methods) showed no microglial activation, while longer exposure to much dimmer cyclic light (25 lux, estimated to produce 250 R* rod^{-1} s^{-1}, Methods) was sufficient to induce microglial activation comparable to that of 200 lux constant light exposure. This shows that retinal microglia activation depends more on light duration than intensity. At no time did we observe a movement of Iba1-positive cells from the outer retina back toward the inner plexiform layer or a return to the highly branched resting state, suggesting that microglia were irreversibly activated on this time scale. Activated microglia did not selectively phagocytose photoreceptor somata that were TUNEL-positive (Fig. 3E), suggesting that the activated microglia engulf indiscriminately, or that the TUNEL signal is an insufficient indicator of cellular demise that attracts microglia. Irreversible activation that might be coupled to non-selective phagocytosis could lead to widespread neuronal tissue loss. Therefore, understanding the mechanisms by which activation can be reversed or phagocytosis can be made selective is a critical step in developing therapies for neurodegenerative disease.

4.2. OCT signals reflect ultrastructural changes in vivo

OCT signals arise from the relative intensity of backscattered light, where the amount of light scattering depends on variations in local optical density and/or refractive index. Thus, OCT images provide clear demarcation of cellular and subcellular boundaries in biological tissue. In the highly layered retinal tissue, the nuclear layers produce relatively low OCT signals, while the synaptic layers, the external limiting membrane, the OS/IS junction and RPE layer produce distinctive bright bands that are relatively consistent across species (McLellan & Rasmussen, 2012). We used OCT to follow light-dependent changes in the Arr1$^{-/-}$ retina, and found a surprising increase in light scattering within the photoreceptor layers (Fig. 2C) on the same time scale (12–48 h) as the migration and activation of the microglia (Fig. 1). In contrast, the standard histological metric for following retinal degeneration, decrease in outer nuclear layer thickness, did not show substantial changes until 72 h (Fig. 3F), the peak time of phagocytosis (Fig. 1). The time course of ONL thinning that we observed by these standard histological measures is similar to the Gnat1-dependent histological changes reported previously (Burns et al., 2006; J. Chen et al., 1999; Hao et al., 2002), though it is important to note that our experiments delivered roughly 100-fold less light to the photoreceptors (200 lux through undilated pupils of pigmented animals, estimated to produce 2000 R* rod^{-1} s^{-1}, Methods). We conclude that the relative intensity of backscattered light shows great promise for earlier detection of cell stress and degeneration, and for measuring such changes in vivo. To our knowledge, this is the first time that changes in OCT-measured light scattering have been quantified across animals, and followed longitudinally within individual animals, in concert with histology and electron microscopy.

OCT is commonly used to measure retinal layer thicknesses in order to follow the progression of retinal degeneration and to evaluate the effectiveness of therapeutic interventions in patient populations. Here we show that OCT measurements of layer thickness are less variable and therefore more sensitive than measurements of ONL layer thickness in histological sections (Fig. 3F). For example, ONL measurements made from both thick (150 μm; green and black circles) and thin (16 μm; blue triangles) fixed sections were more variable than the measures of photoreceptor thickness by OCT (light blue and gray circles) (Fig. 3F). This is not due to the fact that OCT measurements were made from the central retina, because histological measurements showed no significant difference in the change in thickness between the central and peripheral retina (dark blue triangles, Fig. 3F). Instead, the extensive processing

and osmotic changes fixed tissue must undergo likely contribute to sample variability regardless of whether the sections are made 150 μm thick on a vibratome or 16 μm thick on a cryostat. In addition, OCT imaging allows for comparison of the same retinal area in the same mice over time by using the retinal vessels for precise alignment, which surely improves the ability to detect subtle changes in layer thicknesses. This consistency across OCT imaging sessions also lends favorable promise to developing therapeutic interventions in mouse models of retinal degeneration, like the Arr1$^{-/-}$ mouse.

The observed changes in OCT scattering led us to seek ultrastructural correlates with electron microscopy. We observed profound subcellular changes within Arr1$^{-/-}$ photoreceptors by 12 h after light onset, including disruption of the external limiting membrane formed by the adherens junctions of the Müller glial cells with photoreceptor inner segments (Fig. 3A and D, dark arrows). This suggests rapid light-dependent gliosis in the Arr1$^{-/-}$ retina, which may in turn help to stimulate microglial activation and direct radial migration. Because Arr1 plays an essential role in deactivating phototransduction in the rod outer segments, it was somewhat surprising to find the discs and outer segment structure intact following light exposure. Instead, the most severe ultrastructural changes in the Arr1$^{-/-}$ photoreceptors were the highly vesiculated inner segments. In addition, the apoptopedia emanating from the photoreceptor nuclei (Fig. 3C and D) and the perinuclear TUNEL staining (Fig. 3E) was evident at 12–24 h of light exposure, indicating the rapid initiation of photoreceptor cell death.

4.3. Why are microglia not activated by saturating light in normal retinas?

Arr1$^{-/-}$ photoreceptors have been previously shown to undergo apoptosis by two distinct mechanisms: (1) "dim light" degeneration (2000 lux without pupil dilation) and (2) "bright light" degeneration (5000 lux with pupil dilation), which leads to induction of the apoptotic transcription factor, AP-1 (Hao et al., 2002). In previous studies, "dim light"-dependent photoreceptor degeneration in Arr1$^{-/-}$ mice was rescued by concomitant genetic deletion of Gnat1 (Hao et al., 2002), which is essential for light-evoked signaling in rods (Calvert et al., 2000). It has therefore been argued that prolonged phototransduction signaling is an essential first step in Arr1$^{-/-}$ light-dependent degeneration. Indeed, in our experiments, loss of both Gnat1 and Arr1 not only rescued photoreceptor degeneration, but also prevented light-dependent microglial activation and changes in OCT-measured light scattering. Thus, phototransduction is essential for initiating photoreceptor cell stress and microglial activation in this model of light-dependent degeneration.

Why does phototransduction not cause microglial activation in WT retinas, which should also be experiencing continuous rod signaling under these light levels? In the normal mouse retina, bright steady light induces translocation of Arr1 from the inner segments to the outer segments (reviewed in Chen, 2014). In addition, steady light exposure of >1 h causes a 2-fold increase in Arr1 gene expression, which has been correlated with partial recovery of the rod ERG a-wave, a measure of the rod circulating current (Codega et al., 2009). Together, these findings suggest that increased levels of Arr1 in light-adapted WT rods indeed may prevent them from being saturated by the 200 lux illumination in our experiments.

Rod saturation in bright light is expected to dramatically reduce energy expenditure, primarily by removing the burden of ATP-dependent maintenance of electrochemical gradients (Okawa et al., 2008). Consistent with this idea, we find the mitochondria of dark-adapted rods to be highly elongated and positioned directly under the inner segment plasma membrane (Fig. 3A, B, and D). In bright light, the mitochondria of WT rods appear more

numerous and no longer axially oriented, and instead appear to cluster at the base of the outer segment near the site of disc morphogenesis. However, in light-exposed Arr1$^{-/-}$ rods, the mitochondria appear swollen or altogether burst (Fig. 3C). If WT rods escape saturation and Arr1$^{-/-}$ rods do not, as proposed above, Arr1$^{-/-}$ rods should have a larger excess of cellular ATP and lower mitochondrial activity than normal. This reduced mitochondrial activity is expected to result in higher-than-normal oxygen tension and may contribute to oxidative damage of the mitochondria, cytochrome C release and ultimately apoptosis (Geller et al., 2006; Ott et al., 2007).

4.4. Conclusions

In summary, we have shown that microglial activation, proliferation, and migration are initiated by dim light in the Arr1$^{-/-}$ mouse. While the involvement of microglia in light-induced retinal degeneration has been explored in many mouse models, the Arr1$^{-/-}$ mouse is a novel, inducible system for studying the progressive stages of microglial activity across the retina that also avoids confounding inflammatory events like intraocular injection or laser damage, which devastate multiple cell types. Studying microglia in a mouse model where degeneration is tightly controlled will help to determine the factors that regulate the time course of microglial activation and reversibility, and facilitate the testing of potential therapeutic targets to slow or prevent inflammation and retinal degeneration.

Acknowledgments

References

Aguzzi, A., Barres, B. A., & Bennett, M. L. (2013). Microglia: Scapegoat, saboteur, or something else? *Science, 339*(6116), 156–161.

Alam, S., Zawadzki, R. J., Choi, S., Gerth, C., Park, S. S., Morse, L., et al. (2006). Clinical application of rapid serial Fourier-domain optical coherence tomography for macular imaging. *Ophthalmology, 113*(8), 1425–1431.

Burns, M. E., Mendez, A., Chen, C.-K., Almuete, A., Quillinan, N., Simon, M. I., et al. (2006). Deactivation of phosphorylated and nonphosphorylated rhodopsin by arrestin splice variants. *The Journal of Neuroscience, 26*(3), 1036–1044.

Burns, M. E., & Pugh, E. N. J. (2010). Lessons from photoreceptors: Turning off G-protein signaling in living cells. *Physiology, 25*(2), 72–84.

Calvert, P. D., Krasnoperova, N. V., Lyubarsky, a. L., Isayama, T., Nicoló, M., Kosaras, B., et al. (2000). Phototransduction in transgenic mice after targeted deletion of the rod transducin alpha-subunit. *Proceedings of the National Academy of Sciences of the United States of America, 97*(25), 13913–13918.

Chen, J. (2014). The physiological roles of arrestin-1 in rod photoreceptor cells. *Handbook of Experimental Pharmacology, 219*, 85–99.

Chen, C. K., Burns, M. E., Spencer, M., Niemi, G. A., Chen, J., Hurley, J. B., et al. (1999). Abnormal photoresponses and light-induced apoptosis in rods lacking rhodopsin kinase. *Proceedings of the National Academy of Sciences of the United States of America, 96*(7), 3718–3722.

Chen, J., Simon, M. I., Matthes, M. T., Yasumura, D., & LaVail, M. M. (1999). Increased susceptibility to light damage in an arrestin knockout mouse model of Oguchi disease (stationary night blindness). *Investigative Ophthalmology & Visual Science, 40*(12), 2978–2982.

Chiu, S. J., Li, X. T., Nicholas, P., Toth, C. A., Izatt, J. A., & Farsiu, S. (2010). Automatic segmentation of seven retinal layers in SDOCT images congruent with expert manual segmentation. *Optics Express, 18*(18), 19413–19428.

Codega, P., Della Santina, L., Gargini, C., Bedolla, D. E., Subkhankulova, T., Livesey, F. J., et al. (2009). Prolonged illumination up-regulates arrestin and two guanylate cyclase activating proteins: A novel mechanism for light adaptation. *The Journal of Physiology, 587*(Pt 11), 2457–2472.

Daniele, L. L., Insinna, C., Chance, R., Wang, J., Nikonov, S. S., & Pugh, E. N. (2011). A mouse M-opsin monochromat: Retinal cone photoreceptors have increased M-opsin expression when S-opsin is knocked out. *Vision Research, 51*(4), 447–458.

Drexler, W., & Fujimoto, J. G. (2008). State-of-the-art retinal optical coherence tomography. *Progress in Retinal and Eye Research, 27*(1), 45–88.

Duker, J. S., & Adhi, M. (2013). Optical coherence tomography – Current and future applications. *Current Opinion in Ophthalmology, 24*(3), 213–221.

Farhat, G., Mariampillai, A., Yang, V. X. D., Czarnota, G. J., & Kolios, M. C. (2011). Detecting apoptosis using dynamic light scattering with optical coherence tomography. *Journal of Biomedical Optics, 16*(7), 070505.

Geller, S., Krowka, R., Valter, K., & Stone, J. (2006). Toxicity of hyperoxia to the retina: Evidence from the mouse. In J. G. Hollyfield, R. E. Anderson, & M. M. LaVail (Eds.). *Retinal degenerative diseases* (Vol. 3841, pp. 425–437). US: Springer.

Hanisch, U.-K., & Kettenmann, H. (2007). Microglia: Active sensor and versatile effector cells in the normal and pathologic brain. *Nature Neuroscience, 10*(11), 1387–1394.

Hao, W., Wenzel, A., Obin, M. S., Chen, C.-K., Brill, E., Krasnoperova, N. V., et al. (2002). Evidence for two apoptotic pathways in light-induced retinal degeneration. *Nature Genetics, 32*(2), 254–260.

Hume, D. A., Perry, V. H., & Gordon, S. (1983). Immunohistochemical localization of a macrophage-specific antigen in developing mouse retina: Phagocytosis of dying neurons and differentiation of microglial cells to form a regular array in the plexiform layers. *The Journal of Cell Biology, 97*(1), 253–257.

Joly, S., Francke, M., Ulbricht, E., Beck, S., Seeliger, M., Hirrlinger, P., et al. (2009). Cooperative phagocytes: Resident microglia and bone marrow immigrants remove dead photoreceptors in retinal lesions. *The American Journal of Pathology, 174*(6), 2310–2323.

Karlstetter, M., Ebert, S., & Langmann, T. (2010). Microglia in the healthy and degenerating retina: Insights from novel mouse models. *Immunobiology, 215*(9–10), 685–691.

Kettenmann, H., Kirchhoff, F., & Verkhratsky, A. (2013). Microglia: New roles for the synaptic stripper. *Neuron, 77*, 10–18.

Kim, D. Y., Fingler, J., Werner, J. S., Schwartz, D. M., Fraser, S. E., & Zawadzki, R. J. (2011). In vivo volumetric imaging of human retinal circulation with phase-variance optical coherence tomography. *Biomedical Optics Express, 2*(6), 1504–1513.

Langmann, T. (2007). Microglia activation in retinal degeneration. *Journal of Leukocyte Biology, 81*(6), 1345–1351.

Lee, J. Y., Chiu, S. J., Srinivasan, P. P., Izatt, J. A., Toth, C. A., Farsiu, S., et al. (2013). Fully automatic software for retinal thickness in eyes with diabetic macular edema from images acquired by cirrus and spectralis systems. *Investigative Ophthalmology & Visual Science, 54*(12), 7595–7602.

Lyubarsky, A. L., Daniele, L. L., & Pugh, E. N. (2004). From candelas to photoisomerizations in the mouse eye by rhodopsin bleaching in situ and the light-rearing dependence of the major components of the mouse ERG. *Vision Research, 44*(28), 3235–3251.

Mattapallil, M. J., Wawrousek, E. F., Chan, C.-C., Zhao, H., Roychoudhury, J., Ferguson, T., et al. (2012). The Rd8 mutation of the Crb1 gene is present in vendor lines of C57BL/6N mice and embryonic stem cells, and confounds ocular induced mutant phenotypes. *Investigative Ophthalmology & Visual Science, 53*(6), 2921–2927.

McLellan, G. J., & Rasmussen, C. A. (2012). Optical coherence tomography for the evaluation of retinal and optic nerve morphology in animal subjects: Practical considerations. *Veterinary Ophthalmology, 15*(Suppl. 2), 13–28.

Mulvey, C. S., Zhang, K., Bobby Liu, W.-H., Waxman, D. J., & Bigio, I. J. (2011). Wavelength-dependent backscattering measurements for quantitative monitoring of apoptosis, part 2: Early spectral changes during apoptosis are linked to apoptotic volume decrease. *Journal of Biomedical Optics, 16*(11), 117002.

Okawa, H., Sampath, A. P., Laughlin, S. B., & Fain, G. L. (2008). ATP consumption by mammalian rod photoreceptors in darkness and in light. *Current Biology: CB, 18*(24), 1917–1921.

Ott, M., Gogvadze, V., Orrenius, S., & Zhivotovsky, B. (2007). Mitochondria, oxidative stress and cell death. *Apoptosis: An International Journal on Programmed Cell Death, 12*(5), 913–922.

Poon, I. K. H., Chiu, Y.-H., Armstrong, A. J., Kinchen, J. M., Juncadella, I. J., Bayliss, D. A., et al. (2014). Unexpected link between an antibiotic, pannexin channels and apoptosis. *Nature, 507*(7492), 329–334.

Santos, A. M., Martín-Oliva, D., Ferrer-Martín, R. M., Tassi, M., Calvente, R., Sierra, A., et al. (2010). Microglial response to light-induced photoreceptor degeneration in the mouse retina. *The Journal of Comparative Neurology, 518*(4), 477–492.

Van der Meer, F. J., Faber, D. J., Aalders, M. C. G., Poot, A. A., Vermes, I., & van Leeuwen, T. G. (2010). Apoptosis- and necrosis-induced changes in light attenuation measured by optical coherence tomography. *Lasers in Medical Science, 25*(2), 259–267.

Wagner, E., McCaffery, P., & Dräger, U. C. (2000). Retinoic acid in the formation of the dorsoventral retina and its central projections. *Developmental Biology, 222*(2), 460–470.

Wirenfeldt, M., Dissing-Olesen, L., Anne Babcock, A., Nielsen, M., Meldgaard, M., Zimmer, J., et al. (2007). Population control of resident and immigrant microglia by mitosis and apoptosis. *The American Journal of Pathology, 171*(2), 617–631.

Wong, W. T. (2013). Microglial aging in the healthy CNS: Phenotypes, drivers, and rejuvenation. *Frontiers in Cellular Neuroscience, 7*(March), 22.

Xu, J., Dodd, R. L., Makino, C. L., Simon, M. I., Baylor, D. A., & Chen, J. (1997). Prolonged photoresponses in transgenic mouse rods lacking arrestin. *Nature, 389*(October), 505–509.

Yoon, K., & FitzGerald, P. G. (2009). Periplakin interactions with lens intermediate and beaded filaments. *Investigative Ophthalmology & Visual Science, 50*(3), 1283–1289.

Zawadzki, R. J., Jones, S. M., Olivier, S. S., Zhao, M., Bower, B. A., Izatt, J. A., et al. (2005). Adaptive-optics optical coherence tomography for high-resolution and high-speed 3D retinal in vivo imaging. *Optics Express, 13*(21), 8532.